

Bio-therapeutic Potential and Cytotoxicity Assessment of Pectin-Mediated Synthesized Nanostructured Cerium Oxide

Sandeep N. Patil¹ · Jayasinh S. Paradeshi¹ ·
Prapti B. Chaudhari² · Satyendra J. Mishra² ·
Bhushan L. Chaudhari¹

Received: 1 February 2016 / Accepted: 6 May 2016 /
Published online: 27 May 2016
© Springer Science+Business Media New York 2016

Abstract In the present studies, renewable and nontoxic biopolymer, pectin, was extracted from Indian red pomelo fruit peels and used for the synthesis of cerium oxide nanoparticles (CeO₂-NPs) having bio-therapeutic potential. The structural information of extracted pectin was investigated by FTIR and NMR spectroscopic techniques. Physicochemical characteristics of this pectin suggested its application in the synthesis of metal oxide nanoparticles. Using this pectin as a template, CeO₂-NPs were synthesized by simple, one step and eco-friendly approach. The UV–Vis spectrum of synthesized CeO₂-NPs exhibited a characteristic absorption peak at wavelength 345 nm, which can be assigned to its intrinsic band gap (3.59 eV) absorption. Photoluminescence measurements of CeO₂-NPs revealed that the broad emission was composed of seven different bands. FTIR analysis ensured involvement of pectin in the formation and stabilization of CeO₂-NPs. FT-Raman spectra showed a sharp Raman active mode peak at 461.8 cm⁻¹ due to a symmetrical stretching mode of Ce–O vibration. DLS, FESEM, EDX, and XRD analysis showed that the CeO₂-NPs prepared were polydispersed, spherical shaped with a cubic fluorite structure and average particle size ≤40 nm. These CeO₂-NPs displayed broad spectrum antimicrobial activity, antioxidant potential, and non-cytotoxic nature.

Keywords Pectin · Indian red pomelo fruit peels · Cerium oxide nanoparticles · Antioxidant · Antibacterial · Non-cytotoxic

Electronic supplementary material The online version of this article (doi:10.1007/s12010-016-2121-9) contains supplementary material, which is available to authorized users.

✉ Bhushan L. Chaudhari
blchaudhari@nmu.ac.in; blchaudhari@hotmail.com

¹ Department of Microbiology, School of Life Sciences, North Maharashtra University, Umavi Nagar, Post Box 80, Jalgaon 425 001, India

² Department of Polymer Science and Technology, University Institute of Chemical Technology, North Maharashtra University, Jalgaon 425 001, India

Introduction

Nanocrystalline cerium oxide is an important rare earth oxide nanomaterial which has attracted enormous research interest in recent years due to its wide range of applications in various fields, such as catalysis, diesel fuel additives, fuel cells, optical devices, polishing materials, sensors, ultraviolet absorbers, sun screen cosmetics, and biomedical science fields [1–8]. Several physical and chemical approaches exist for the synthesis of cerium oxide nanoparticles (CeO_2 -NPs), including hydrolysis, hydrothermal, microwave assisted, wet chemical, electrochemical, sol–gel, etc. [9, 10]. However, these methods involved either the use of organic solvents or templating agents that are potentially harmful to the environment as well as biological systems [11].

In recent years, more attention is being paid towards synthesis of nanoparticles with the naturally abundant green materials which are renewable, eco-friendly and cost-effective [12]. Biopolymers from natural sources such as starch, agarose, chitosan, gelatin, and gum tragacanth have been exploited for the synthesis of nanoceria [12–16]. Pectins are soluble non-starch polysaccharides extracted from the primary cell walls of plants and anionic in nature. These are made up of linear 1, 4-linked D-galacturonic acid and are heterogeneous complex polysaccharides [17, 18]. Like other biopolymers, pectin has also an ability to serve as a reliable stabilizing agent for metal oxide nanoparticles. Up till now, several studies have demonstrated the ability of pectin in the synthesis of silver, gold, ZnO, CuS, and hydroxyapatite nanoparticles as an appropriate stabilizing and capping agent [19–24]. However, to the best of our knowledge, no report exists on the pectin-mediated synthesis of CeO_2 -NPs.

Commercial extraction of pectin can be achieved from apple pomace, diverse citrus products, for example, orange and passion fruit in placidly acidic conditions [17]. The composition of the pectin molecule depends on its source. For example, pectin from citrus fruits usually contains less neutral sugars and higher degree of esterification [25]. The presence of carboxyl groups in pectin is a favorable factor for using this material in facial nanomaterial synthesis [20].

Red pomelo (*Citrus maxima*) is the biggest fruit among the citrus species and a popular fruit crop of the Orient including India. For 2008, the top ten world producers of *Citrus maxima* (including pomelo) are USA, China, Mexico, South Africa, India, Argentina, Turkey, Cuba, Brazil, and Tunisia [26]. In 2010–2011, total world production of pomelo was 6385 metric tons across the world where India stands fifth having production of 198,000 metric tons per year [27]. The inner sweet pulp of the fruit is usually eaten or used for making juices or wines, whereas the outer peels are discarded as waste [26]. As the peels of citrus fruits are usually rich in pectin [25], peels of red pomelo can be used as a raw material for the extraction of pectin which will add value to the agro-waste.

Keeping this background in mind, the present study was carried out with two main objectives: (i) to establish peels of red pomelo (agro/food waste) as an alternative source for industrial pectin production and (ii) to propose application of this pectin in the green synthesis of therapeutically important CeO_2 -NPs. Therefore, in the present work, pectin was extracted from peels of red pomelo (*Citrus maxima*). It was characterized for physicochemical properties and used for the synthesis of CeO_2 -NPs. After the synthesis, CeO_2 -NPs were characterized for their structural and optical properties. Further, CeO_2 -NPs were evaluated for biological potentials such as anti-bacterial effects, antioxidant activities, and erythrocyte cytotoxicity.

Materials and Methods

All chemicals used were purchased from either Sigma (Bangalore) or Himedia (Mumbai) and were of analytical grade with high quality and purity.

Preparation of raw Material for Pectin Extraction

Indian red pomelo (*Citrus maxima*) was purchased from a local fruit market. The peels were stripped with a paring knife. The red pomelos were thoroughly washed with water to remove any dirt and other macroscopic contaminants. Flavedo (yellowish green peel) was removed by manual shaving. Then, their albedos (inner spongy white peel) were separated from the pomelo fruits. Albedos were cut into a cube size approximately $5 \times 5 \times 5 \text{ mm}^3$. The albedos were soaked in water for overnight to wash out water-soluble substances followed by soaking in methanol to remove polyphenols present, if any. The pre-soaked albedos were dried at $50 \text{ }^\circ\text{C}$ in a hot-air oven to obtain a constant weight. The dried pomelo albedos were crushed, and then screened through a sieve of 60-mesh size to get particles which were further used as a raw material for pectin extraction.

Extraction of Pectin

Pectin extraction was performed by microwave-assisted extraction process [28]. A domestic microwave oven (GMS 17 M 07 WHGX Godrej, India), at working frequency 2450 MHz and maximum power output 900 W, with adjustable microwave power and irradiation time was used for extraction. The albedos flour (5 g) was added to 150 ml water and pH of the mix was adjusted to 2.5 with HCl (0.1 N) as extracting agent. Then, it was heated in the microwave oven (power of 0.9 kW) for 6 min. Later, upon cooling, the mixture was separated by centrifuging at 2000 rpm for 20 min. The pH of the supernatant was adjusted to 4.5 with NaOH (0.1 N) followed by addition of equal volume of 96 % ethanol to it and allowed to stand. After 6 h of incubation, the coagulated mass was observed which was separated by centrifugation and washed twice with 96 % ethanol. It was dried at $50 \text{ }^\circ\text{C}$ in a laboratory drier. Subsequently, the dried powder was separated and was finally freeze-dried at $-50 \text{ }^\circ\text{C}$ for 48 h.

Characterization of Extracted Pectin

The physical properties such as swelling index and effective pore radius were determined by following the method of Goel et al. [29]. The chemical properties like equivalent weight, methoxyl content, acetyl value, anhydrouronic acid, and degree of esterification of extracted pectin were determined by the titration methods [30]. The apparent viscosity of pectin solution (1.0 % w/v prepared in 0.1 N NaCl) was determined using a viscometer (model RV DV-1 Brookfield, USA) with a speed of 50 rpm at $25 \text{ }^\circ\text{C}$. This apparent viscosity was converted to relative viscosity and intrinsic viscosity (supplementary information) of Indian red pomelo pectin (IRP-P). The molecular weight of IRP-P was estimated by applying the Mark–Houwink–Sakurada equation as suggested by Arslan which relates intrinsic viscosity with molecular weight [31]. The structural information of IRP-P was investigated by ^1H and ^{13}C NMR spectroscopy.

Synthesis of CeO₂-NPs Using Pectin

A solution was prepared by dissolving 0.2 g of IRP-P in 100 ml of deionized distilled water and stirred for 10 min at 60 °C. A 50 mL of 0.5 M cerium nitrate solution was added to the pectin solution gradually under vigorous stirring for 30 min at 60 °C. An excess amount of liquid ammonia was added in a drop-wise manner until the pH of the solution reached to 10. The solution was allowed to stir for an hour. Initially, the color of the solution was light yellow which later changed to yellow with increase in ammonia concentration. The yellow-colored precipitate obtained was centrifuged and washed several times with acetone and subsequently with water to make it free from nitrate, ammonia, and organic impurities. The washed precipitate was dried at 60 °C for 12 h which was then annealed at 400 °C for 4 h and subjected to characterization. The sample was stored in desiccator for further studies.

Characterization of CeO₂-NPs

The optical absorption properties of synthesized material were determined using double beam UV–vis spectrophotometer (UV-1800, Shimadzu, Japan) over the range of 200–800 nm. The photoluminescence (PL) emission spectrum was recorded with fluorescence spectrophotometer (RF5301PC, Shimadzu, Japan) at an excitation wavelength of 320 nm. Its FT-Raman analysis was done using the stand alone FT-Raman Spectrometer (RSF-27, Bruker, Germany) excited with an Nd:YAG laser (1064 nm) using laser power of 100 mW within the scan range of 50–1500 cm⁻¹. Possible functional groups involved in the synthesis of nanoparticles were determined by FTIR spectrometer (Spectrum Two, FTIR-88522, Perkin Elmer, USA). The surface morphology and the elemental analysis of synthesized CeO₂-NPs were analyzed by field emission scanning electron microscopy (FESEM) and energy-dispersive X-ray spectroscopy (EDX) using instrument FESEM (S4800 Type II, Hitachi, Japan) equipped with EDX (X flash detector-5030, Bruker, Germany). The particle size and stability of CeO₂-NPs (dispersed in deionized water by sonication) was determined using Zeta-sizer (NanoZS-9, Malvern, UK) instrument. The XRD pattern was obtained with 2θ varying from 20 to 80° with an X-ray diffractometer (D8-Advance, Bruker, Germany) with CuKα₁ radiation (λ=1.5404 Å) to obtain the crystal phase information of CeO₂-NPs.

Evaluation of Antioxidant Potential of CeO₂-NPs

The antioxidant activity of CeO₂-NPs was determined by 2, 2-diphenyl-1-picrylhydrazyl (DPPH) radical scavenging assays [32]. Initially, the stability of DPPH solution was confirmed by keeping the DPPH solution undisturbed for 2 h in the dark and change in color was observed and its absorbance at 517 nm was measured. In a typical process, 10 mL DPPH solution in ethanol (0.2 mg/mL) was taken in an amber-colored glass bottle, and an appropriate aliquot of well-dispersed CeO₂-NPs stock prepared in ethanol was added so as to obtain a final concentration to 4 mg/mL of CeO₂-NPs. The gradual change in color from deep violet to pale yellow due to scavenging of free DPPH radicals was monitored at 517 nm with different time intervals. DPPH radical scavenging activity was also calculated by varying

concentration of CeO₂-NPs (0.5 to 8.0 mg/mL) for 1 h and expressed in terms of percentage of DPPH radical scavenged as calculated below.

$$\% \text{DPPH radical scavenged} = \frac{(\text{OD Control} - \text{OD Test})}{\text{OD Control}} \times 100$$

where, OD is the optical density measured at 517 nm.

Evaluation of Antibacterial Activity of CeO₂-NPs

Antibacterial potential of CeO₂-NPs was measured against *Bacillus subtilis* (ATCC 6633) and *Escherichia coli* (ATCC 8739) strains by using a colony-forming capability test as described by Lu et al. [33]. Cultures were inoculated in a 50-mL Luria-Bertani (LB) medium independently and cultured with constant shaking (120 rpm) at 37 °C overnight.

These cultures were exposed to different concentrations of CeO₂-NPs by transferring 5 mL of culture suspension to the tubes containing 5 mL of sterile suspension of CeO₂-NPs in LB broth to get a final CeO₂-NPs concentrations of 1 and 2 mM. The mixture was incubated at 37 °C for 4 h. After incubation, 100 μL of appropriate dilutions of bacterial suspensions was spread onto LB agar plates. These plates were allowed to incubate at 37 °C in the dark overnight and the colony-forming unit (CFU) of the treated bacterial suspension was counted. For comparison purpose, treatment sets with similar concentrations of cerium nitrate and bulk cerium oxide were also run. The negative control set with only sterile LB broth (devoid of any cerium compound) was also run. The survival percentage of bacteria was used to evaluate the antimicrobial effects of the CeO₂-NPs, cerium nitrate and bulk cerium oxide as calculated with the following equation:

$$\% \text{Survival} = \frac{\text{CFU of treated bacterial culture}}{\text{CFU of control bacterial culture}} \times 100$$

Cytotoxicity Assessment of CeO₂-NPs

Cytotoxicity of CeO₂-NPs towards normal human cells was evaluated by erythrocyte hemolysis assay [34]. Blood from a healthy volunteer was collected by using a syringe. To inhibit the coagulation of blood, 0.5 mL of 0.3 % EDTA solution was mixed to 9.5 mL of the blood. It was then centrifuged at 1000 rpm for 10 min to remove the supernatant containing platelets and plasma. The pellet containing erythrocytes was re-suspended in 10 mL of phosphate-buffered saline (PBS) having pH 7.4 and the process was repeated three times. Finally, the cells were suspended in PBS to get a uniform cell suspension having 5 % (v/v) density. The 2 mL of erythrocyte suspension was added to each tube. The appropriate aliquots of CeO₂-NPs solution from well-dispersed CeO₂-NPs stock prepared in PBS were added in different tubes to obtain the desired concentrations. The tubes were inverted and gently shaken to maintain contact of the erythrocytes with the nanoparticles and incubated at 37 °C for 1 h. The sterile deionized water was used as a positive

control while PBS acted as a negative control. After incubation, the samples were centrifuged at 3000 rpm for 5 min to pellet out the RBCs. The absorption of the supernatant was measured at 540 nm against the appropriate blank. The percent hemolysis relative to positive control was calculated for each sample as below.

$$\% \text{Hemolysis} = \frac{(\text{OD test sample} - \text{OD negative control})}{(\text{OD positive control} - \text{OD negative control})} \times 100$$

where, OD is the optical density measured at 540 nm.

Results and Discussion

Extraction and Characterization of Pectin from Indian Red Pomelo Peels

Indian red pomelo peels after soaking in water followed by methanol and drying in hot air oven yielded around 28.43 % raw material for extraction of pectin. The microwave-assisted extraction process yielded around 29.37 % (w/w) of pure pectin from this raw material after freeze-drying. Dried apple pomace and citrus peels are commercially used raw materials for extraction of pectin with yields of 15.20 and 30.35 % [35, 36]. The results of present studies revealed that the yield of Indian red pomelo pectin (IRP-P) were comparable to these commercial sources, thus, suggesting it as an alternative source for industrial pectin production.

The physical and chemical properties of IRP-P are listed in Table 1. The IRP-P showed high methoxy content (11.30 ± 0.46), therefore, higher degree of esterification (79.04 ± 0.7 %). This high degree of esterification favors the synthesis of nanoparticles [20]. The apparent viscosity of IRP-P solution (0.5 % w/v in 0.1 N, NaCl) at 25 °C was 1.61 ± 0.03 Pa s. The relative and intrinsic viscosities of this IRP-P solution were 1.66 ± 0.03 and 1.32 ± 0.06 . The molecular weight estimated from viscosity was 36.495 KDa.

The chemical structure of IRP-P studied by ^1H and ^{13}C NMR spectra. In ^1H NMR spectrum of IRP-P (Fig. S1), the signals at 1.16 and 1.31 ppm can be attributed to methyl groups of L-rhamnose. Two signals at 1.99 and 2.12 could be assigned to

Table 1 Physical and chemical properties of extracted IRP-P

Sr. No.	Parameters	Results	
1	Swelling index in	HCl (0.1 N)	1.56 ± 0.24
		Buffer pH 4	2.86 ± 0.32
		Buffer pH 7	3.41 ± 0.28
		Buffer pH 10	4.87 ± 0.31
2	Effective pore radius in mm	$4.13 \pm 0.24 \times 10^{-1}$	
3	Equivalent weight	1183.4 ± 15.7	
4	Methoxyl content (%)	11.30 ± 0.46	
5	Acetyl value (%)	0.34 ± 0.07	
6	Anhydrouronic acid content (%)	81.17 ± 2.66	
7	Degree of esterification (%)	79.04 ± 0.71	

acetyl groups attached to D-galacturonic acid [37]. The chemical shifts of protons H-1, H-2, H-3, H-4, and H-5 of α -galacturonosyl residues appeared as prominent signals at 5.30, 3.97, 3.95, 4.12 and 4.71 ppm [38]. In ^{13}C NMR spectrum of IRP-P (Fig. S2), the chemical shifts were determined for D-galacturonic acid. The signals located at 16.64 and 174.61 ppm are characteristic signals of carboxyl-bonded methyl groups (CH_3 -6) of galactopyranosyl residues and free carboxyl group of galacturonic acid, respectively [24]. The major signals located at 103.62, 76.31, 73.91, 72.50, 71.00, and 60.03 could be assigned to C-1, C-4, C-5, C-2, C-3, and C-6 of 1, 4-linked D-galactopyranose residues, respectively [38]. The ^1H and ^{13}C NMR signals clearly indicated the presence of the backbone chain of 1, 4-linked D-galacturonic acid along with branches at various positions in the IRP-P. This structural characterization of IRP-P confirmed the presence of esterified pectin having a potential for being used in the synthesis of nanomaterials.

Pectin-Assisted Synthesis of CeO_2 -NPs

The pectin acts as a reducing agent and undergoes destructive changes during synthesis of nanoparticles [19]. The carboxy, hydroxyl, and keto functional groups of pectin fragments participate in formation of nanoparticles [39]. The possible mechanism involved in the formation of CeO_2 -NPs is shown in Fig. 1. In the alkaline medium, pectin undergoes transformations such as depolymerization, alkaline hydrolysis, and oxidizing destruction leading to produce monomers, galacturonic acid [19]. In alkaline pectin solution, oxygen atoms of the OH branches of galacturonic acid attract the metal cations from cerium nitrate added to the reaction mixture [13]. The nitrates (from precursor cerium nitrate) present in the solution get decomposed due to heating to form nitrogen dioxide and oxygen and get released from the reaction mixture [40]. After addition of liquid ammonia to the reaction mixture, hydration of Ce^{+3} ions to $\text{Ce}(\text{OH})_3$ take place which further get precipitated out due to its

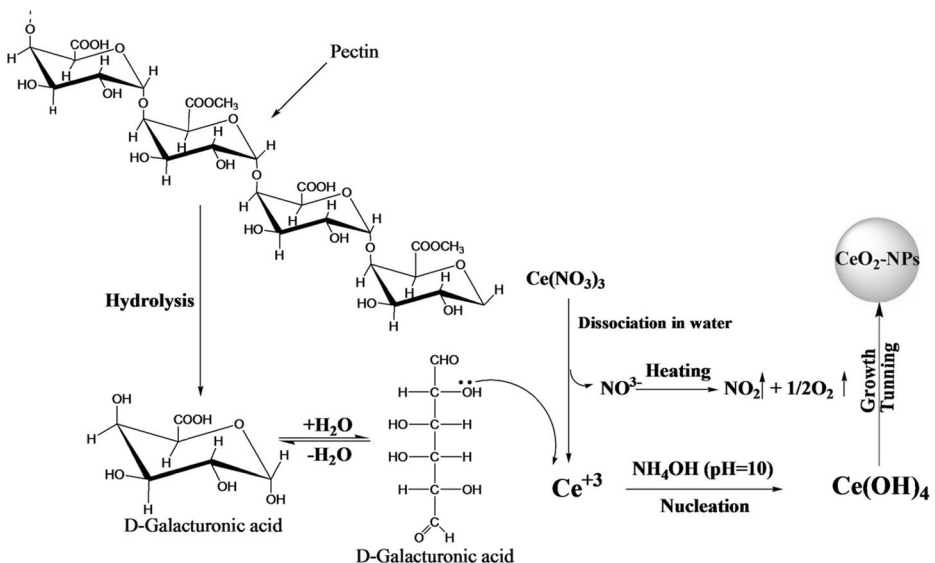


Fig. 1 Probable mechanism of pectin-mediated synthesis of CeO_2 -NPs

extremely low-solubility constant [41]. After precipitation, the surplus alkaline environment results into oxidation of $\text{Ce}(\text{OH})_3$ to $\text{Ce}(\text{OH})_4$, i.e., $[\text{Ce}^{3+}]$ to $[\text{Ce}^{4+}]$. This shift causes a change in color of the solution from colorless to light yellow. The hydroxyl ions seem to play an important role in the yellow-colored precipitation, subsequent oxidation of Ce(III) to Ce(IV), and further formation of CeO_2 -NPs [42]. The final heat treatment (calcination) provides enough energy necessary for dehydrative conversion of $\text{Ce}(\text{OH})_4$ into cerium oxide (CeO_2) and further growth of highly crystallized CeO_2 -NPs.

Spectroscopic and Microscopic Characterization of CeO_2 -NPs

UV–vis Spectrum

The UV–vis spectrum of CeO_2 -NPs exhibited a characteristic absorption peak at wavelength 345 nm (Fig. 2a). This can be assigned to an intrinsic band gap absorption of CeO_2 -NPs due to the electron transitions from the valence band [O(2p)] to the conduction band [Ce(4f)] in CeO_2 -NPs [12].

By fitting of UV–vis absorption data to the direct transition equation and extrapolating the linear portions of the curves to absorption equal to zero (Fig. 2b), the band gap of CeO_2 -NPs

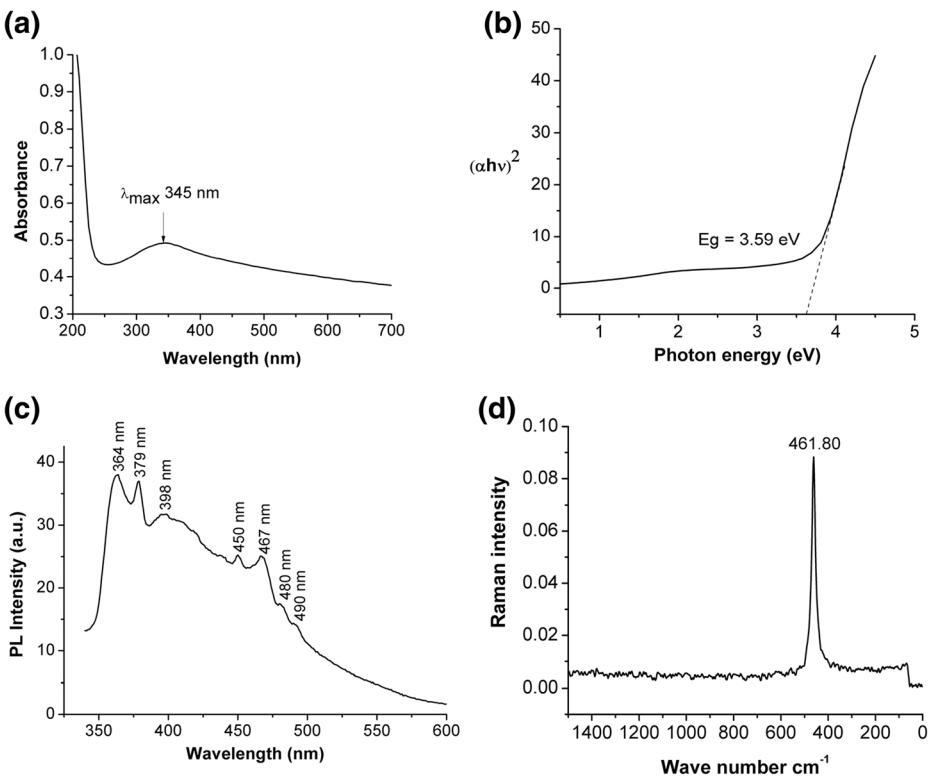


Fig. 2 a UV–vis spectrum. b Photon energy level. c Photoluminescence spectrum recorded under 320-nm light excitation wavelength. d Raman spectrum of pectin-mediated synthesized CeO_2 -NPs

was estimated as 3.59 eV, which is 0.40 eV more than the reported band gap value of bulk CeO_2 powders (3.19 eV) [43]. This increase in band gap can be attributed to the quantum confinement effect caused due to reduction in particle size to a few nanometers [44] or the charge transition of Ce ion (Ce^{3+} to Ce^{4+}) [11].

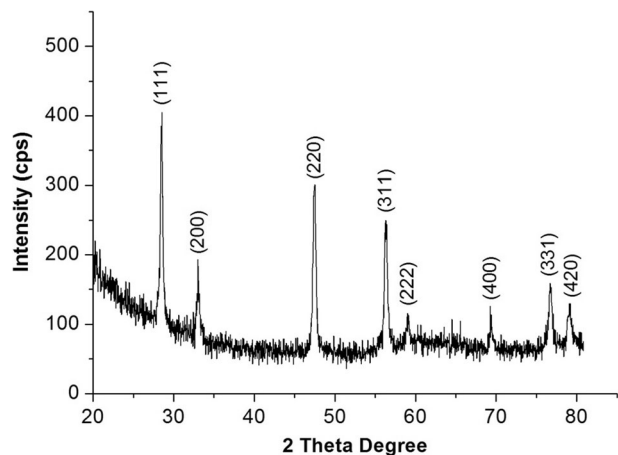
Photoluminescence (PL) Spectrum

The photoluminescence (PL) spectrum of the CeO_2 -NPs was measured for an excitation wavelength equal to 320 nm (Fig. 2c). The PL spectrum of CeO_2 -NPs displayed several strong emission bands from very a short wavelength of 360 nm to a very long wavelength of 500 nm. The emission spectra showed three peaks (364, 379, and 398 nm) in the near band edge emission region and four peaks (450 and 467, 480 and 490 nm) in the blue-green region of visible range. The emission peaks at 364, 379, and 398 nm can be related to the band-to-band recombination process, possibly involving localized or free excitons [45]. Two blue emission peaks at 450 and 467 nm can be related to the hopping of electrons from the localized [Ce(4f)] state to the [O(2p)] valence band [46]. Two green emission peaks at 480 and 490 nm are possible due to surface defects in the CeO_2 -NPs, and the low density of oxygen vacancies may be the reason for their weaker intensities. Similar kinds of results were reported for the CeO_2 -NPs synthesized by using *Gloriosa superba* leaf extract and cationic surfactant; CTAB [11, 47].

Raman Spectrum

The formation of a cubic structure in the synthesized CeO_2 -NPs was further supported by Raman spectrum of CeO_2 -NPs (Fig. 2d). A Raman active mode with strong and broadening peak was found at 461.1 cm^{-1} , which can be attributed to a symmetrical stretching mode of the Ce–O8 vibration unit [48].

Fig. 3 X-ray powdered diffraction pattern of pectin-mediated synthesized CeO_2 -NPs



XRD Analysis

The XRD patterns of pectin mediated synthesized CeO₂-NPs (annealed) is shown in Fig. 3. The Bragg peaks are located at angle (2θ) of 28.51, 33.06, 47.42, 56.30, 59.09, 69.00, 76.57, and 78.99 ° with Miller indices (111), (200), (220), (311), (222), (400), (331), and (420), respectively. These peaks can be indexed to a pure cubic fluorite structure of CeO₂-NPs (space group: Fm-3 m, 225), which are in agreement with the Joint Committee for Powder Diffraction Standards-powder diffraction file for CeO₂ (JCPDS PDF 00-033-0334). The value of lattice constant *a* for CeO₂-NPs was 5.089 Å and the unit cell volume calculated from the relation $V=a^3$ was found to be 131.795 Å³. The average crystallite size of the CeO₂-NPs was estimated as 23.71 nm using Debye Scherrer equation.

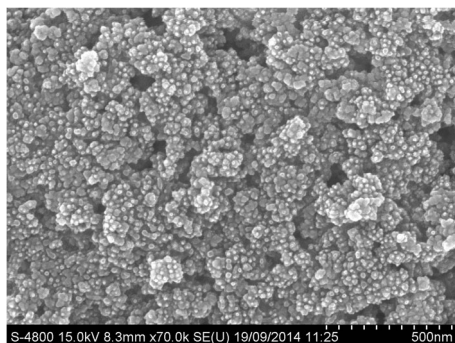
FESEM and EDX Analysis

The FESEM micrograph of CeO₂-NPs synthesized by using pectin as a stabilizing and reducing agent is shown in Fig. 4. The CeO₂-NPs were spherical in shape, but it seemed to be agglomerated and their apparent size was ranging from 5 to 40 nm. The EDX pattern of CeO₂-NPs clearly showed the presence of Ce, O, C and Au as main constituents in the structure of as-synthesized CeO₂-NPs nanoparticles (Fig. S3). The presence of Ce and O in the atomic ratio of 11:25 (almost 1:2) confirmed the CeO₂ in the structure, C appeared due to carbon conductive tape used to hold the specimen and Au appeared due to gold coating of sample before FESEM and EDX analysis.

Particle Size Analysis and Stability Study

The particle size distribution histogram of CeO₂-NPs (Fig. 5) confirmed the hydrodynamic size (Z-average) of CeO₂-NPs to be 29.47 nm. The corresponding average zeta potential value of these nanoparticles was -28.0 mV with good quality, indicating the stability of CeO₂-NPs (Fig. S4).

Fig. 4 Field emission scanning electron micrograph of pectin-mediated synthesized CeO₂-NPs



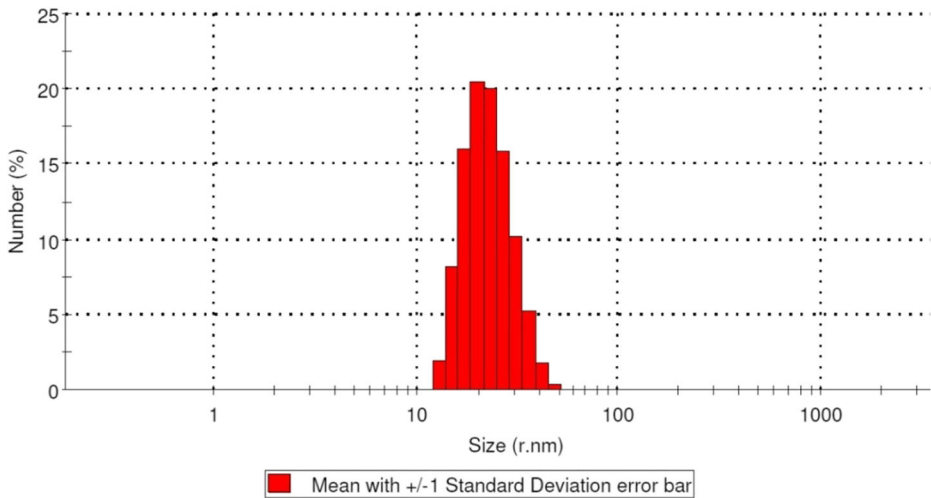
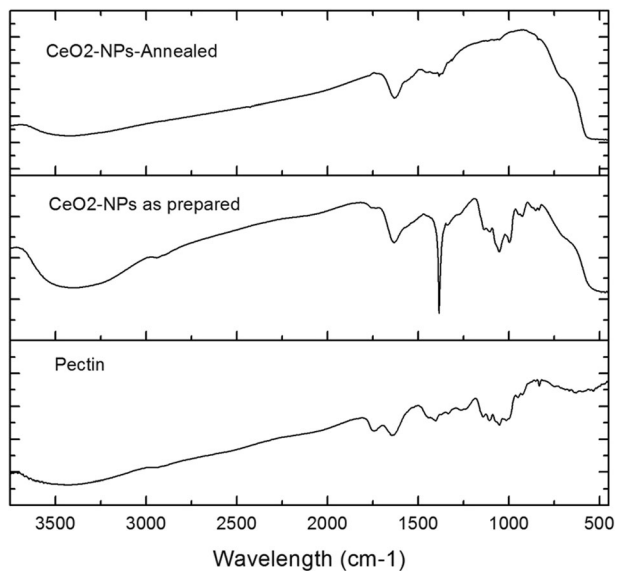


Fig. 5 Particle size distribution histogram of pectin-mediated synthesized CeO_2 -NPs

FTIR Spectroscopic Analysis

The FTIR spectra of pectin, pectin-mediated synthesized CeO_2 -NPs (as prepared), and CeO_2 -NPs annealed are shown Fig. 6. The FTIR spectrum of IRP-P showed the presence of characteristic peaks at 3390, 2939, 1738, 1634, 1402, 1295, 1105, 1051, and 955 cm^{-1} which could be assigned to the stretching frequency of -OH group, C-H stretching of the methyl esters of galacturonic acid, C=O stretching vibration of the methyl esterified carboxyl groups,

Fig. 6 FTIR spectrum of pectin, pectin-mediated synthesized CeO_2 -NPs (as prepared) and CeO_2 -NPs annealed



C=O stretching vibration of ionic carboxyl groups, vibration of the C–O–H in plane bending, asymmetric C–O–C stretching vibration of -O-CH₃ (methoxyl) groups, bending modes of acetal (COCOC) groups, bending modes of etheral (COC) groups, and glycosidic group, respectively [23]. Similar type of peaks were observed in the FTIR spectrum of as-synthesized CeO₂-NPs, along with additional sharp peak at 545 cm⁻¹ which is the typical peak for the Ce–O stretching vibration and is characteristic phonon mode for cubic cerium oxide [49]. The sharp band at 1384 cm⁻¹ could be due to N=O stretching vibration indicating traces of nitrate [50]. In the FTIR spectrum of annealed CeO₂-NPs, a typical very sharp peak for Ce–O stretching vibration at 558 cm⁻¹ was observed along with peaks at 3397, 1624, and 1471 cm⁻¹ which were accountable for water and CO₂ taken up from the environment [51].

Antioxidative Potential of CeO₂-NPs

The DPPH radical scavenging assay is considered to be one of the most widespread and promising techniques for evaluating the antioxidative potential of materials. In the current studies also, DPPH radical scavenging assay was used to evaluate of antioxidant activity of CeO₂-NPs. After keeping DPPH solution under dark, there was no change of color as well as the absorption intensity at 517 nm which confirmed the stability of DPPH solution during the experiment. The color of DPPH solution gradually changed from deep violet to pale yellow in the presence of CeO₂-NPs. With time, peak intensity at 517 nm gradually decreased (Fig. 7a). This decrease in the peak intensity provides the direct evidence for the free radical scavenging capacity of CeO₂-NPs. In the current studies, the DPPH radical scavenging capacity of CeO₂-NPs (4.0 mg/mL) was up to 73.36 % in 60 min. With increase in the concentration of CeO₂-NPs, the peak intensity was decreased at a faster rate (Fig. 7b). The IC-50 value calculated for DPPH radical scavenging potential of CeO₂-NPs was 1.83 mg/mL.

In nanoform, cerium oxide has a fluorite crystalline structure bearing unique antioxidant properties resulting from the kinetics and thermodynamics of the redox processes occurring at the surface of nanoparticles [52]. CeO₂-NPs display both catalase and superoxide dismutase mimetic activity which provide the ability to regenerate its antioxidant activity [7, 9].

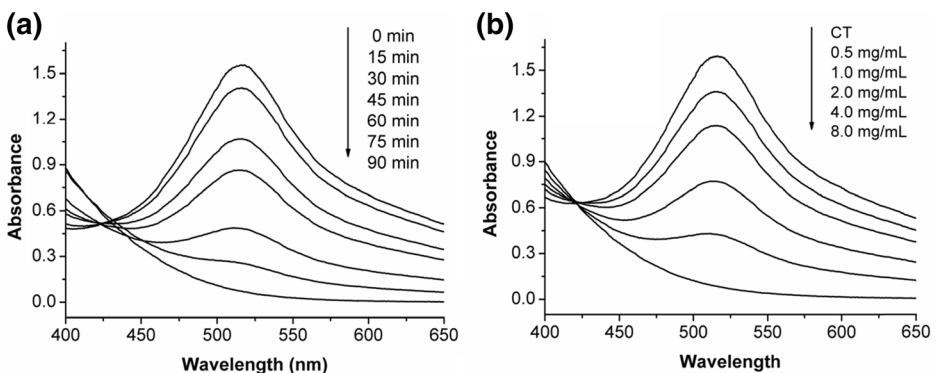
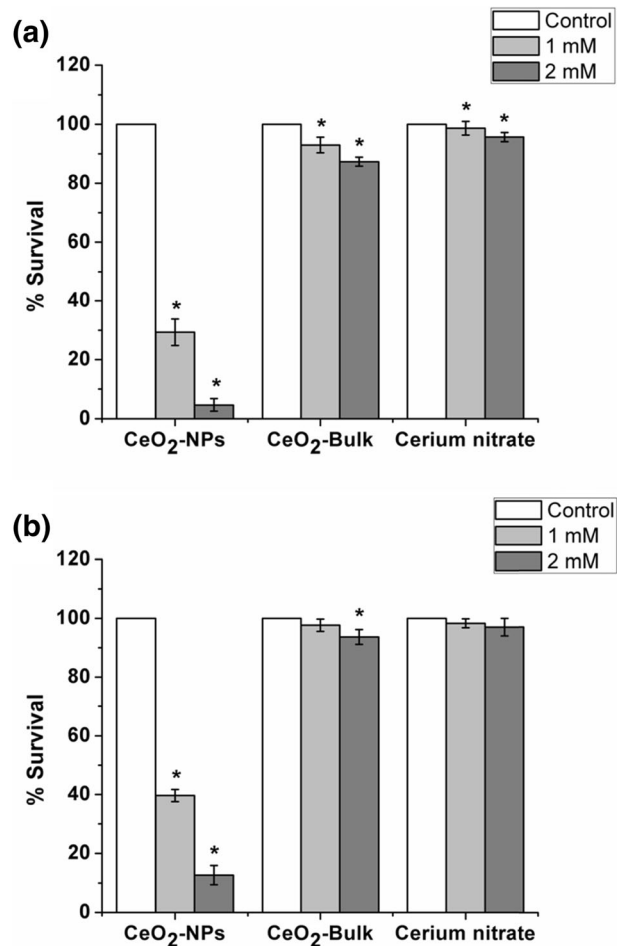


Fig. 7 Antioxidant activity of CeO₂-NPs assessed by DPPH radical scavenging assay at **a** different time intervals and **b** different concentrations

Fig. 8 Antibacterial activity of CeO₂-NPs, CeO₂-Bulk and cerium nitrate against **a** *E. coli* and **b** *B. subtilis*, expressed in terms of percentage of the survival relative to the control group. In a group, the bars not labeled with an asterisk indicate values (means) are significantly different from the control ($p \leq 0.05$) by Dunnett's comparison test



Antibacterial Potential of CeO₂-NPs

The synthesized CeO₂-NPs exhibited broad-spectrum antibacterial activity against both Gram-positive (*B. subtilis*) and Gram-negative (*E. coli*) bacteria. The antimicrobial activity of synthesized CeO₂-NPs, bulk CeO₂ powder, and cerium nitrate at two different concentrations (1 and 2 mM) is shown in Fig. 8. The CeO₂-NPs at 1 mM concentration possessed antibacterial potential against both bacteria which increased further on increasing the concentration. The CeO₂-NPs showed better activity against *E. coli* than *B. subtilis* at both concentrations tested which might be due to structural difference in the cell wall of these bacteria. The results suggested that antibacterial activity of CeO₂-NPs against both the bacteria was much greater than that of bulk CeO₂ powder and cerium nitrate. Similar kinds of results were noted by Kuang et al. [53]. Exposure of bulk CeO₂ powder and cerium nitrate (at concentrations of 1 and 2 mM) to *E. coli* caused significant decrease ($p \leq 0.05$) in survival

Table 2 Cytotoxicity of CeO₂-NPs measured by erythrocyte hemolysis assay

Sr. No.	Sample	Optical density at 540 nm	Percentage hemolysis
1	Distilled water	1.658 ± 0.028	100 (positive control)
2	Physiological saline	0.034 ± 0.003	0 (negative control)
3	CeO ₂ -NPs (0.50 mg/mL)	0.043 ± 0.003	0.55
4	CeO ₂ -NPs (1.00 mg/mL)	0.051 ± 0.006	1.05
5	CeO ₂ -NPs (2.00 mg/mL)	0.069 ± 0.005	2.16
6	CeO ₂ -NPs (4.00 mg/mL)	0.108 ± 0.008	4.55
7	CeO ₂ -NPs (8.00 mg/mL)	0.169 ± 0.008	8.31

as compared to control (Fig. 8a). In case of *B. subtilis*; cerium nitrate was not found effective at both the concentrations (1 and 2 mM) and bulk CeO₂ showed slight reduction in survival at 2 mM concentration only (Fig. 8b). The antibacterial activity of *Aspergillus niger* culture filtrate mediated synthesized cerium oxide nanoparticles was also reported against *E. coli*, *Proteus vulgaris*, *Streptococcus pneumonia* and *B. subtilis* [54].

The exact mechanism behind the antibacterial activity of CeO₂-NPs is unclear; however, in general: (i) membrane damage due to uneven surface of these nanoparticles, (ii) their interactions with membrane bound mesosomes and thiol groups (–SH) of the membrane proteins leading to disturbance in the cellular respiration and nutrient transport, and (iii) their binding with DNA leading to altered DNA replication and cell division, etc. could be the possible reasons [55–57].

Cytotoxicity Assessment by Erythrocyte Hemolysis Assay

In order to assess biocompatibility of metallic or metal oxide nanoparticles initially, erythrocyte hemolysis assay is usually carried out. Hemolysis basically relates to the release of hemoglobin into the plasma due to the damage of erythrocyte membrane [58]. The permissible limit of hemolysis set for biocompatibility assessment of material/biomaterial is 5 % [59]. The results of erythrocyte hemolysis by CeO₂-NPs are summarized in the Table 2.

Overall, less hemolysis was observed for CeO₂-NPs. Hemolysis increased with increasing the concentrations of CeO₂-NPs. In the present studies, CeO₂-NPs showed hemolysis within the permissible limit at a concentration ≤4 mg/mL. Thus, it can be said that the synthesized CeO₂-NPs are biocompatible in nature; but the concentration of CeO₂-NPs >4 mg/mL may not be safe for human beings.

Conclusion

In the present work, extraction of biopolymer pectin from Indian red pomelo fruit peels and its use in synthesis of CeO₂-NPs was successfully done. The spectroscopic and microscopic characterization revealed the formation of CeO₂-NPs morphology with the average particle size ≤40 nm. The synthesized CeO₂-NPs possessed potent antioxidant and antibacterial activity. Additionally, these nanoparticles proved to be biocompatible. The synthesis of these CeO₂-NPs can certainly be an ecofriendly and facile approach using natural material.

Acknowledgment SNP and JSP are thankful to the UGC, New Delhi for UGS-BSR/RFSMS fellowships. PBC is grateful to the DST, New Delhi for INSPIRE fellowship. All the authors acknowledge the SAIF-Chandigarh for NMR spectroscopic analysis, SAIF-IIT Chennai for FT-Raman spectroscopic study and UGS-SAP-DRS III and DST-FIST for providing infrastructure at School of Life Sciences of North Maharashtra University, Jalgaon.

References

- Kockrick, E., Schrage, C., Grigas, A., Geiger, D., & Kaskel, S. (2008). Synthesis and catalytic properties of microemulsion-derived cerium oxide nanoparticles. *Journal of Solid State Chemistry*, *181*(7), 1614–1620.
- Selvan, V. A. M., Anand, R. B., & Udayakumar, M. (2009). Effects of cerium oxide nanoparticle addition in diesel and diesel–biodiesel–ethanol blends on the performance and emission characteristics of a CI engine. *Journal of Engineering and Applied Science*, *4*(7), 1819–6608.
- Jacobs, G., Williams, L., Graham, U., Thomas, G. A., Sparks, D. E., & Davis, B. H. (2003). Low temperature water–gas shift: in situ DRIFTS-reaction study of ceria surface area on the evolution of formates on Pt/CeO₂ fuel processing catalysts for fuel cell applications. *Applied Catalysis A: General*, *252*(1), 107–118.
- Kaittanis, C., Santra, S., Asati, A., & Perez, J. M. (2012). A cerium oxide nanoparticles based device for the detection of chronic inflammation via optical and magnetic resonance imaging. *Nanoscale*, *4*(6), 2117–2123.
- Khan, S. B., Faisal, M., Rahman, M. M., & Jamal, A. (2011). Exploration of CeO₂ nanoparticles as a chemi-sensor and photo-catalyst for environmental applications. *Science of the Total Environment*, *409*(15), 2987–2992.
- Yabe, S., & Sato, T. (2003). Cerium oxide for sunscreen cosmetics. *Journal of Solid State Chemistry*, *171*(1), 7–11.
- Celardo, I., Pedersen, J. Z., Traversa, E., & Ghibelli, L. (2011). Pharmacological potential of cerium oxide nanoparticles. *Nanoscale*, *3*(4), 1411–1420.
- Das, S., Dowding, J. M., Klump, K. E., McGinnis, J. F., Self, W., & Seal, S. (2013). Cerium oxide nanoparticles: applications and prospects in nanomedicine. *Nanomedicine*, *8*(9), 1483–1508.
- Soren, S., Jena, S. R., Samanta, L., & Parhi, P. (2015). Antioxidant potential and toxicity study of the cerium oxide nanoparticles synthesized by microwave-mediated synthesis. *Applied Biochemistry and Biotechnology*, *177*(1), 148–161.
- Sun, C., Li, H., & Chen, L. (2012). Nanostructured ceria-based materials: synthesis, properties, and applications. *Energy & Environmental Science*, *5*(9), 8475–8505.
- Arumugam, A., Karthikeyan, C., Hameed, A. S. H., Gopinath, K., Gowri, S., & Karthika, V. (2015). Synthesis of cerium oxide nanoparticles using *Gloriosa superba* L. leaf extract and their structural, optical and antibacterial properties. *Materials Science and Engineering: C*, *49*, 408–415.
- Kargar, H., Ghasemi, F., & Darroudi, M. (2015). Bioorganic polymer-based synthesis of cerium oxide nanoparticles and their cell viability assays. *Ceramics International*, *41*(1), 1589–1594.
- Darroudi, M., Sarani, M., Oskuee, R. K., Zak, A. K., Hosseini, H. A., & Gholami, L. (2014). Green synthesis and evaluation of metabolic activity of starch mediated nanoceria. *Ceramics International*, *40*(1), 2041–2045.
- Sifontes, A. B., Gonzalez, G., Ochoa, J. L., Tovar, L. M., Zoltan, T., & Canizales, E. (2011). Chitosan as template for the synthesis of ceria nanoparticles. *Materials Research Bulletin*, *46*(11), 1794–1799.
- Darroudi, M., Hakimi, M., Sarani, M., Oskuee, R. K., Zak, A. K., & Gholami, L. (2013). Facile synthesis, characterization, and evaluation of neurotoxicity effect of cerium oxide nanoparticles. *Ceramics International*, *39*(6), 6917–6921.
- Darroudi, M., Sarani, M., Oskuee, R. K., Zak, A. K., & Amiri, M. S. (2014). Nanoceria: gum mediated synthesis and in vitro viability assay. *Ceramics International*, *40*(2), 2863–2868.
- Rolin, C. (2002). 8 Commercial pectin preparations. In G. B. Seymour & J. P. Knox (Eds.), *Pectins and their manipulation* (1st ed., pp. 222–223). Oxford: Blackwell.
- Rangel-Rodríguez, A. M., Conxita, S., Susana, V., Flores-Gallardo, S. G., Contreras-Esquivel, J. C., & Licea-Jiménez, L. (2014). Immobilization of pectinesterase in genipin-crosslinked chitosan membrane for low methoxyl pectin production. *Applied Biochemistry and Biotechnology*, *174*(8), 2941–2950.
- Zahrán, M. K., Ahmed, H. B., & El-Rafie, M. H. (2014). Facile size-regulated synthesis of silver nanoparticles using pectin. *Carbohydrate Polymers*, *111*, 971–978.
- Nigoghossian, K., dos Santos, M. V., Barud, H. S., da Silva, R. R., Rocha, L. A., Caiut, J. M., de Assuncao, R. M. N., Spanhele, L., Poulain, M., Messaddeq, Y., & Ribeiro, S. J. (2015). Orange pectin mediated growth and stability of aqueous gold and silver nanocolloids. *Applied Surface Science*, *341*, 28–36.
- Wang, A. J., Liao, Q. C., Feng, J. J., Zhang, P. P., Li, A. Q., & Wang, J. J. (2012). Apple pectin-mediated green synthesis of hollow double-caged peanut-like ZnO hierarchical superstructures and photocatalytic applications. *CrystEngComm*, *14*(1), 256–263.

22. Gupta, V. K., Pathania, D., Agarwal, S., & Singh, P. (2012). Adsorptional photocatalytic degradation of methylene blue onto pectin–CuS nanocomposite under solar light. *Journal of Hazardous Materials*, *243*, 179–186.
23. Gopi, D., Kanimozhi, K., Bhuvaneshwari, N., Indira, J., & Kavitha, L. (2014). Novel banana peel pectin mediated green route for the synthesis of hydroxyapatite nanoparticles and their spectral characterization. *Spectrochimica Acta Part A: Molecular and Biomolecular Spectroscopy*, *118*, 589–597.
24. Gopi, D., Kanimozhi, K., & Kavitha, L. (2015). Opuntia ficus indica peel derived pectin mediated hydroxyapatite nanoparticles: synthesis, spectral characterization, biological and antimicrobial activities. *Spectrochimica Acta Part A: Molecular and Biomolecular Spectroscopy*, *141*, 135–143.
25. Kravtchenko, T. P., Voragen, A. G. J., & Pilnik, W. (1992). Analytical comparison of three industrial pectin preparations. *Carbohydrate Polymers*, *18*(1), 17–25.
26. Online: Crop Info and How-To Guide in Growing Pummelo. Available from: www.cropsreview.com/pummelo.html. Accessed 21 Apr 2016.
27. Online: C I T R U S: Statistics - fresh and processed citrus fruit. Available from: www.fao.org/fileadmin/templates/est/COMM_MARKETS_MONITORING/Citrus/Documents/CITRUS_BULLETIN_2012.pdf. Accessed 21 Apr 2016.
28. Bagherian, H., Ashtiani, F. Z., Fouladitajar, A., & Mohtashamy, M. (2011). Comparisons between conventional, microwave-and ultrasound-assisted methods for extraction of pectin from grapefruit. *Chemical Engineering and Processing: Process Intensification*, *50*(11), 1237–1243.
29. Goel, H., Kaur, G., Tiwary, A. K., & Rana, V. (2010). Formulation development of stronger and quick disintegrating tablets: a crucial effect of chitin. *Yakugaku Zasshi*, *130*(5), 729–735.
30. Jindal, M., Kumar, V., Rana, V., & Tiwary, A. K. (2013). *Aegle marmelos* fruit pectin for food and pharmaceuticals: physico-chemical, rheological and functional performance. *Carbohydrate Polymers*, *93*(2), 386–394.
31. Arslan, N. (1995). Extraction of pectin from sugar-beet pulp and intrinsic viscosity molecular weight relationship of pectin solutions. *Journal of Food Science and Technology-Mysore*, *32*(5), 381–385.
32. Das, D., Nath, B. C., Phukon, P., & Dolui, S. K. (2013). Synthesis of ZnO nanoparticles and evaluation of antioxidant and cytotoxic activity. *Colloids and Surfaces B: Biointerfaces*, *111*, 556–560.
33. Lu, Z., Mao, C., Meng, M., Liu, S., Tian, Y., Yu, L., Sun, B., & Li, C. M. (2014). Fabrication of CeO₂ nanoparticle-modified silk for UV protection and antibacterial applications. *Journal of Colloid and Interface Science*, *435*, 8–14.
34. Kumar, K. P., Paul, W., & Sharma, C. P. (2011). Green synthesis of gold nanoparticles with *Zingiber officinale* extract: characterization and blood compatibility. *Process Biochemistry*, *46*(10), 2007–2013.
35. Visser, J., & Voragen, A. G. J. (Eds.). (1996). Pectins and pectinases. In *Progress in Biotechnology* (pp. 3–19). Amsterdam: Elsevier Science.
36. Da Silva, J. L., & Rao, M. A. (2006). 11 pectins: structure, functionality, and uses. In A. M. Stephen, G. O. Phillips, & P. A. Williams (Eds.), *Food polysaccharides and their applications* (2nd ed., pp. 353–397). New York: CRC Press.
37. Tamaki, Y., Uechi, S., Taira, T., Ishihara, M., Adaniya, S., Uesato, K., Fukuda, M., & Tako, M. (2004). Isolation and characterization of pectin from pericarp of *Citrus depressa*. *Journal of Applied Glycoscience*, *51*(1), 19–25.
38. Habibi, Y., Heyraud, A., Mahrouz, M., & Vignon, M. R. (2004). Structural features of pectic polysaccharides from the skin of *Opuntia ficus-indica* prickly pear fruits. *Carbohydrate Research*, *339*(6), 1119–1127.
39. Ivanova, N. V., Trofimova, N. N., Es'kova, L. A., & Babkin, V. A. (2012). The study of the reaction of Pectin-Ag (0) nanocomposites formation. *International Journal of Carbohydrate Chemistry*. doi:10.1155/2012/459410.
40. Zak, A. K., Majid, W. A., Mahmoudian, M. R., Darroudi, M., & Yousefi, R. (2013). Starch-stabilized synthesis of ZnO nanopowders at low temperature and optical properties study. *Advanced Powder Technology*, *24*(3), 618–624.
41. Sohnel, O., & Garside, J. (1992). *Precipitation: Basic principles and industrial applications*. Butterworth-Heinemann.
42. Chen, H. I., & Chang, H. Y. (2004). Homogeneous precipitation of cerium dioxide nanoparticles in alcohol/water mixed solvents. *Colloids and Surfaces A: Physicochemical and Engineering Aspects*, *242*(1), 61–69.
43. Orel, Z. C., & Orel, B. (1994). Optical properties of pure CeO₂ and mixed CeO₂/SnO₂ thin film coatings. *Physica Status Solidi B*, *186*(1), K33–K36.
44. Tsunekawa, S., Wang, J. T., Kawazoe, Y., & Kasuya, A. (2003). Blueshifts in the ultraviolet absorption spectra of cerium oxide nanocrystallites. *Journal of Applied Physics*, *94*(5), 3654–3656.
45. Wang, L., Ren, J., Liu, X., Lu, G., & Wang, Y. (2011). Evolution of SnO₂ nanoparticles into 3D nanoflowers through crystal growth in aqueous solution and its optical properties. *Materials Chemistry and Physics*, *127*(1), 114–119.

46. Sun, C., Li, H., Zhang, H., Wang, Z., & Chen, L. (2005). Controlled synthesis of CeO₂ nanorods by a solvothermal method. *Nanotechnology*, *16*(9), 1454.
47. Wang, G., Mu, Q., Chen, T., & Wang, Y. (2010). Synthesis, characterization and photoluminescence of CeO₂ nanoparticles by a facile method at room temperature. *Journal of Alloys and Compounds*, *493*(1), 202–207.
48. George, S., Pokhrel, S., Xia, T., Gilbert, B., Ji, Z., Schowalter, M., Rosenauer, A., Damoiseaux, R., Bradley, K. A., Mädler, L., & Nel, A. E. (2009). Use of a rapid cytotoxicity screening approach to engineer a safer zinc oxide nanoparticle through iron doping. *ACS Nano*, *4*(1), 15–29.
49. Wang, A. Q., D'Souza, N., & Golden, T. D. (2006). Electrosynthesis of nanocrystalline cerium oxide/layered silicate powders. *Journal of Materials Chemistry*, *16*(5), 481–488.
50. Darroudi, M., Hoseini, S. J., Oskuee, R. K., Hosseini, H. A., Gholami, L., & Gerayli, S. (2014). Food-directed synthesis of cerium oxide nanoparticles and their neurotoxicity effects. *Ceramics International*, *40*(5), 7425–7430.
51. Khan, S. B., Faisal, M., Rahman, M. M., Akhtar, K., Asiri, A. M., Khan, A., & Alamry, K. A. (2013). Effect of particle size on the photocatalytic activity and sensing properties of CeO₂ nanoparticles. *International Journal of Electrochemical Science*, *8*, 7284–7297.
52. Korsvik, C., Patil, S., Seal, S., & Self, W. T. (2007). Superoxide dismutase mimetic properties exhibited by vacancy engineered ceria nanoparticles. *Chemical Communications*, *14*(10), 1056–1058.
53. Kuang, Y., He, X., Zhang, Z., Li, Y., Zhang, H., Ma, Y., Wu, Z., & Chai, Z. (2011). Comparison study on the antibacterial activity of nano-or bulk-cerium oxide. *Journal of Nanoscience and Nanotechnology*, *11*(5), 4103–4108.
54. Gopinath, K., Karthika, V., Sundaravadivelan, C., Gowri, S., & Arumugam, A. (2015). Mycogenesis of cerium oxide nanoparticles using *Aspergillus niger* culture filtrate and their applications for antibacterial and larvicidal activities. *Journal of Nanostructure in Chemistry*, *5*(3), 295–303.
55. Stoimenov, P. K., Klinger, R. L., Marchin, G. L., & Klabunde, K. J. (2002). Metal oxide nanoparticles as bactericidal agents. *Langmuir*, *18*(17), 6679–6686.
56. Tong, G. X., Du, F. F., Liang, Y., Hu, Q., Wu, R. N., Guan, J. G., & Hu, X. (2013). Polymorphous ZnO complex architectures: selective synthesis, mechanism, surface area and Zn-polar plane-codetermining antibacterial activity. *Journal of Materials Chemistry B*, *1*(4), 454–463.
57. Hajipour, M. J., Fromm, K. M., Ashkarran, A. A., de Aberasturi, D. J., de Laramendi, I. R., Rojo, T., Serpooshan, V., Parak, W. J., & Mahmoudi, M. (2012). Antibacterial properties of nanoparticles. *Trends in Biotechnology*, *30*(10), 499–511.
58. Sharp, M. K., & Mohammad, S. F. (1998). Scaling of hemolysis in needles and catheters. *Annals of Biomedical Engineering*, *26*(5), 788–797.
59. Singhal, J. P., & Ray, A. R. (2002). Synthesis of blood compatible polyamide block copolymers. *Biomaterials*, *23*(4), 1139–1145.